Available online at www.sciencedirect.com
ScienceDirect
Journal of Computational Physics 217 (2006) 453–472
JOURNAL OF COMPUTATIONAL PHYSICS
www.elsevier.com/locate/jcp

Accuracy study of the IDO scheme by Fourier analysis

Yohsuke Imai *, Takayuki Aoki

Global Scientific Information and Computing Center, Tokyo Institute of Technology, 2-12-1O-okayama, Meguro-ku, Tokyo 152-8550, Japan

Received 24 May 2005; received in revised form 31 October 2005; accepted 7 January 2006
Available online 21 February 2006

Abstract

The numerical accuracy of the Interpolated Differential Operator (IDO) scheme is studied with Fourier analysis for the solutions of Partial Differential Equations (PDEs): advection, diffusion, and Poisson equations. The IDO scheme solves governing equations not only for physical variable but also for first-order spatial derivative. Spatial discretizations are based on Hermite interpolation functions with both of them. In the Fourier analysis for the IDO scheme, the Fourier coefficients of the physical variable and the first-order derivative are coupled by the equations derived from the governing equations. The analysis shows the IDO scheme resolves all the wavenumbers with higher accuracy than the fourth-order Finite Difference (FD) and Compact Difference (CD) schemes for advection equation. In particular, for high wavenumbers, the accuracy is superior to that of the sixth-order Combined Compact Difference (CCD) scheme. The diffusion and Poisson equations are also more accurately solved in comparison with the FD and CD schemes. These results show that the IDO scheme guarantees highly resolved solutions for all the terms of fluid flow equations.

PACS: 02.60.−x; 02.60.Cb; 02.70.Rw

Keywords: IDO scheme; Numerical accuracy; Fourier analysis; High resolution; Numerical stability; Computational fluid dynamics

1. Introduction

A great number of numerical schemes have been developed for solving Partial Differential Equations (PDEs). Numerical calculations must solve accurately all the wave scales corresponding to the solution of PDE. Most numerical schemes show to converge to the PDE solution by reducing grid spacing, but computer resources such as memory and CPU time are limited. In many cases, a range of wavenumber resolved on given meshes results to be critical.

The spectral method [1] gives the most accurate solutions, and have been used for Direct Numerical Simulation (DNS) of turbulence [2,3]. The application of the spectral method is, however, limited to flows with

* Corresponding author. Tel.: +81 3 5734 3575; fax: +81 3 5734 3276.
E-mail address: yimai@sim.gsic.titech.ac.jp (Y. Imai).

0021-9991/$ - see front matter
doi:10.1016/j.jcp.2006.01.015

periodic boundary conditions, and is not suitable for the steep gradient profiles describing discontinuity within the assigned wavenumber. Finite Difference (FD) schemes used on spatial grid points are easily applied to complex boundaries with less computational cost. The most familiar discretization methods are the first-order forward or backward difference and the second-order central difference. The first- and the second-order derivatives of PDEs are represented by linear combinations of the variables of two or three grid points. Although the calculation of such simple FD scheme has been used for various analysis, very small grid spacing is often required to compensate the low accuracy of the methods.

The classical approach to construct higher-order scheme is to introduce additional grid points in the discretization, that is, the use of five grid point variables makes a fourth-order representation of the first-order derivative, and sixth-order discretization is obtained by referring to seven grid points. These non-compact schemes can therefore present difficulties in dealing with boundary conditions, and furthermore a range of the resolved wavenumber is still narrow. It would be desirable in this regard to develop higher-order schemes based on different approaches. The standard Padê scheme is one example of these approaches. Lele generalized the standard Padê scheme as the Compact finite Difference (CD) scheme [4], and showed that the CD scheme possesses higher resolution than the conventional FD schemes. Another approach that should be mentioned is the Cubic Interpolated Propagation/Constrained Interpolation Profile (CIP) scheme, which is a Semi-Lagrangian hyperbolic equation solver [5,6]. Multi-moments, i.e. not only physical variables but also first-order derivatives, are time integrated as dependent variables, and the spatial profiles of the variables are approximated by the Hermite interpolation function. Utsumi et al. [7] showed that the CIP scheme produces less dissipative solution with smaller phase error than the conventional schemes for advection calculations. The CIP scheme has been extended to the Conservative Semi-Lagrangian (CIP–CSL) scheme [8,9], the Finite Volume formulation (CIP–FVM) [10], the Basis Set (CIP–BS) scheme [11], and the CIP method of Characteristics [12]. In almost all the CIP type schemes, a fractional steps method is introduced for fluid flow simulations, where advection term is solved by the semi-Lagrange way with high accuracy and non-advection term is advanced with the second-order FD scheme.

We have developed the Interpolated Differential Operator (IDO) scheme [13] which is a multi-moment Eulerian scheme. The IDO scheme solves the given PDE straightforwardly, without fractional steps method, and extracts full performance of the Hermite interpolation function constructed by physical variables and first-order derivatives. The major difference between the CD scheme and the IDO scheme is the calculation for the first-order derivatives. While in the CD scheme derivatives at each grid point are implicitly given by the relation matrix to neighboring grid points, the first-order derivatives of the IDO scheme are given as the solution of additional equations derived from governing equations.

The IDO scheme has shown promising results in compressible and incompressible fluid flow problems, in comparison with existing schemes [14,15]. The approximately comparable result has been achieved to that of spectral methods for DNS of homogeneous isotropic turbulence [16]. However, the detailed accuracy and stability of the IDO scheme still remains unclear.

In this paper, we present the accuracy and stability of the IDO scheme by using Fourier analysis. The analysis for the solution of advection, diffusion, and Poisson equations shows that the IDO scheme has higher resolution characteristics than the FD and CD schemes.

2. Review of the IDO scheme

2.1. Spatial discretization

In the IDO scheme, the physical variable f and its first-order spatial derivative f_x are defined at a grid point j as f_j and $f_{x,j}$ in the case of one-dimensional computational domain of $0 = x_0 < x_1 < \cdots < x_{j-1} < x_j < x_{j+1} < \cdots < x_{N-1} < x_N = L$. Owing to the first-order derivative of an additional dependent variable, we solve the additional equation derived by differentiating the given PDE. The higher-order derivatives $f_{xx}(x), f_{xxx}(x), \ldots$ of the PDE are represented as $f_{xx}(x) = F_{xx}(x), f_{xxx}(x) = F_{xxx}(x), \ldots$ by using the Hermite interpolation function $F(x)$, which is constructed by both the physical variables and the first-order derivatives.

Two kinds of interpolation functions, covering different domains, are selectively applied. One interpolation function is a fifth-order polynomial covering the local area from grid point $j-1$ to $j+1$,

$$F(X) = aX^5 + bX^4 + cX^3 + dX^2 + f_{x,j}X + f_j, \tag{2.1}$$

where $X = x - x_j$. The coefficients of the interpolation function are determined by the constraints of $F(h_p) = f_{j+1}$, $F_x(h_p) = f_{x,j+1}$, $F(-h_m) = f_{j-1}$, and $F_x(-h_m) = f_{x,j-1}$, where $h_p = x_{j+1} - x_j$ and $h_m = x_j - x_{j-1}$. In the case of an uniform grid spacing $h_p = h_m = L/N = h$, spatial derivatives at the grid point j are represented by the following expressions:

$$f_{xx}(x_j) = \frac{2}{h^2}(f_{j+1} - 2f_j + f_{j-1}) - \frac{1}{2h}(f_{x,j+1} - f_{x,j-1}), \tag{2.2}$$

$$f_{xxx}(x_j) = \frac{15}{2h^3}(f_{j+1} - f_{j-1}) - \frac{3}{2h^2}(f_{x,j+1} + 8f_{x,j} + f_{x,j-1}), \tag{2.3}$$

$$f_{xxxx}(x_j) = -\frac{12}{h^4}(f_{j+1} - 2f_j + f_{j-1}) + \frac{6}{h^3}(f_{x,j+1} - f_{x,j-1}), \tag{2.4}$$

$$f_{xxxxx}(x_j) = -\frac{90}{h^5}(f_{j+1} - f_{j-1}) + \frac{30}{h^4}(f_{x,j+1} + 4f_{x,j} + f_{x,j-1}). \tag{2.5}$$

A different interpolation function, called upwind interpolation function, is often applied to the advection term of fluid equations for numerical stability. In the same manner of the CIP scheme, the third-order polynomial,

$$F(X) = aX^3 + bX^2 + f_{x,j}X + f_j, \tag{2.6}$$

is used to cover the one-cell in the upwind direction. Using the constraints $F(h') = f_{jup}$ and $F_x(h') = f_{x,jup}$, derivatives at the grid point j are obtained as

$$f_{xx}(x_j) = -\frac{6}{h'^2}(f_j - f_{jup}) - \frac{2}{h'}(2f_{x,j} + f_{x,jup}), \tag{2.7}$$

$$f_{xxx}(x_j) = \frac{12}{h'^3}(f_j - f_{jup}) + \frac{6}{h'^2}(f_{x,j} + f_{x,jup}), \tag{2.8}$$

where $X = x - x_j$, $h' = x_{jup} - x_j$, $jup = j - u/|u|$, u represents advection velocity.

2.2. Time integration

In order to demonstrate time integration method, we consider the following PDE in time and space:

$$f_t = \varphi(f, f_x, f_{xx}, f_{xxx}, \ldots), \tag{2.9}$$

where the subscript t denotes the time derivative. We solve the additional equation derived by differentiating Eq. (2.9) for time integrating the first-order derivative:

$$f_{tx} = \varphi_x(f, f_x, f_{xx}, f_{xxx}, \ldots). \tag{2.10}$$

Both the equations are simultaneously time integrated. The Runge–Kutta time integration method is usually adopted in the IDO scheme to retain high-order accuracy in time. The detailed expressions to integrate Eqs. (2.9) and (2.10) are as follows:

$$k_j^p = \varphi(f^p(x_j), f_x^p(x_j), f_{xx}^p(x_j), f_{xxx}^p(x_j), \ldots), \tag{2.11}$$

$$k_{x,j}^p = \varphi_x(f^p(x_j), f_x^p(x_j), f_{xx}^p(x_j), f_{xxx}^p(x_j), \ldots), \tag{2.12}$$

$$f_j^p = f_j^n + \sum_q \alpha_{pq} k_j^q \Delta t, \tag{2.13}$$

$$f_{x,j}^p = f_{x,j}^n + \sum_q \alpha_{pq} k_{x,j}^q \Delta t, \tag{2.14}$$

$$f_j^{n+1} = f_j^n + \sum_p \beta_p k_j^p \Delta t, \tag{2.15}$$

$$f_{x,j}^{n+1} = f_{x,j}^n + \sum_p \beta_p k_{x,j}^p \Delta t, \tag{2.16}$$

where k^p is the time derivatives in the stage number p of the Runge–Kutta method, α_{pq} and β_p are weighted coefficients, and n is the time step index. The spatial derivatives in Eqs. (2.11) and (2.12) are represented by linear combinations of the set $(f_{j-1}^p, f_j^p, f_{j+1}^p, f_{x,j-1}^p, f_{x,j}^p, f_{j+1}^p)$ through the derivative approximations (2.2)–(2.5), (2.7) and (2.8). In this paper, the following coefficients of α_{pq} and β_p are used:

For the one-stage method, being identical to the first-order finite difference in time:

$$p = 1, \quad \alpha_{11} = 0, \quad \beta_1 = 1. \tag{2.17}$$

For the two-stage method:

$$p = 1, 2, \quad \begin{pmatrix} \alpha_{11} & \alpha_{12} \\ \alpha_{21} & \alpha_{22} \end{pmatrix} = \begin{pmatrix} 0 & 0 \\ 1 & 0 \end{pmatrix}, \quad \begin{pmatrix} \beta_1 \\ \beta_2 \end{pmatrix} = \begin{pmatrix} 1/2 \\ 1/2 \end{pmatrix}. \tag{2.18}$$

For the three-stage method:

$$p = 1, 2, 3, \quad \begin{pmatrix} \alpha_{11} & \alpha_{12} & \alpha_{13} \\ \alpha_{21} & \alpha_{22} & \alpha_{23} \\ \alpha_{31} & \alpha_{32} & \alpha_{33} \end{pmatrix} = \begin{pmatrix} 0 & 0 & 0 \\ 2/3 & 0 & 0 \\ 0 & 2/3 & 0 \end{pmatrix}, \quad \begin{pmatrix} \beta_1 \\ \beta_2 \\ \beta_3 \end{pmatrix} = \begin{pmatrix} 1/4 \\ 3/8 \\ 3/8 \end{pmatrix}. \tag{2.19}$$

For the four-stage method:

$$p = 1, 2, 3, 4,$$
$$\begin{pmatrix} \alpha_{11} & \alpha_{12} & \alpha_{13} & \alpha_{14} \\ \alpha_{21} & \alpha_{22} & \alpha_{23} & \alpha_{24} \\ \alpha_{31} & \alpha_{32} & \alpha_{33} & \alpha_{34} \\ \alpha_{41} & \alpha_{42} & \alpha_{43} & \alpha_{44} \end{pmatrix} = \begin{pmatrix} 0 & 0 & 0 & 0 \\ 1/2 & 0 & 0 & 0 \\ 0 & 1/2 & 0 & 0 \\ 0 & 0 & 1 & 0 \end{pmatrix}, \quad \begin{pmatrix} \beta_1 \\ \beta_2 \\ \beta_3 \\ \beta_4 \end{pmatrix} = \begin{pmatrix} 1/6 \\ 1/3 \\ 1/3 \\ 1/6 \end{pmatrix}. \tag{2.20}$$

3. Fourier analysis for the IDO scheme

3.1. Spatial derivatives in Fourier analysis

When the spatial profile of a dependent variable $f(x)$ is periodic over the domain $[0, L]$ with an uniform grid spacing $h = L/N$, the dependent variable is decomposed into Fourier series,

$$f(x) = \sum_k \hat{f}(k) \mathrm{e}^{\mathrm{i}wx/h}, \tag{3.1}$$

where $\mathrm{i} = \sqrt{-1}$, and $w = 2\pi kh/L$ is a scaled wavenumber. In the IDO scheme, first-order derivative is solved independently, and the spatial profile of the first-order derivative is defined as

$$f_x(x) = \sum_k \hat{f}_x(k) \mathrm{e}^{\mathrm{i}wx/h}. \tag{3.2}$$

The physical variable and the first-order derivative at a grid point j and those of grid points $j \pm 1$ are given by

$$f_j = f(x_j) = \sum_k \hat{f}(k) \mathrm{e}^{\mathrm{i}wx_j/h}, \tag{3.3}$$

$$f_{x,j} = f_x(x_j) = \sum_k \hat{f}_x(k) \mathrm{e}^{\mathrm{i}wx_j/h}, \tag{3.4}$$

$$f_{j\pm1} = f(x_j \pm h) = \sum_k \hat{f}(k) \mathrm{e}^{\mathrm{i}wx_j/h} \mathrm{e}^{\pm \mathrm{i}w}, \tag{3.5}$$

$$f_{x,j\pm1} = f_x(x_j \pm h) = \sum_k \hat{f}_x(k) e^{iwx_j/h} e^{\pm iw}. \tag{3.6}$$

Substituting Eqs. (3.3)–(3.6) into the derivative approximations (2.2)–(2.5) of the fifth-order central interpolation function, we derive the mth-order derivatives represented by the Fourier series:

$$f_{(m)}(x_j) = \sum_k \hat{f}_{(m)}(k) e^{iwx_j/h} = \sum_k A_{(m)}(w) \hat{f}(k) e^{iwx_j/h} + \sum_k A'_{(m)}(w) \hat{f}_x(k) e^{iwx_j/h}, \tag{3.7}$$

where $A_{(m)}$ and $A'_{(m)}$ are determined as follows:

For the second-order derivative:

$$A_{(2)}(w) = 4\frac{\cos w - 1}{h^2}, \quad A'_{(2)}(w) = -i\frac{\sin w}{h}. \tag{3.8}$$

For the third-order derivative:

$$A_{(3)}(w) = 15i\frac{\sin w}{h^3}, \quad A'_{(3)}(w) = -3\frac{\cos w + 4}{h^2}. \tag{3.9}$$

For the fourth-order derivative:

$$A_{(4)}(w) = -24\frac{\cos w - 1}{h^4}, \quad A'_{(4)}(w) = 12i\frac{\sin w}{h^3}. \tag{3.10}$$

For the fifth-order derivative:

$$A_{(5)}(w) = -180i\frac{\sin w}{h^5}, \quad A'_{(5)}(w) = 60\frac{\cos w + 2}{h^4}. \tag{3.11}$$

In the case of derivative approximations (2.7) and (2.8) of the third-order upwind interpolation function, they are represented by

For the second-order derivative:

$$A_{(2)}(w) = 6\frac{e^{iw} - 1}{h^2}, \quad A'_{(2)}(w) = -2\frac{e^{iw} + 2}{h}. \tag{3.12}$$

For the third-order derivative:

$$A_{(3)}(w) = -12\frac{e^{iw} - 1}{h^3}, \quad A'_{(3)}(w) = 6\frac{e^{iw} + 1}{h^2}, \tag{3.13}$$

where advection velocity is a negative constant.

3.2. Time integration in Fourier analysis

We derive the general analysis method for the IDO scheme in solving a linear time dependent PDE,

$$f_t = \varphi(f, f_x, f_{xx}, f_{xxx}, \ldots, f_{(m)}) = \varphi_0 f + \varphi_1 f_x + \varphi_2 f_{xx} + \varphi_3 f_{xxx} + \cdots + \varphi_{(m)} f_{(m)}, \tag{3.14}$$

and its differentiated equation,

$$f_{tx} = \varphi_x(f, f_x, f_{xx}, f_{xxx}, \ldots, f_{(m)}) = \varphi_0 f_x + \varphi_1 f_{xx} + \varphi_2 f_{xxx} + \varphi_3 f_{xxxx} + \cdots + \varphi_{(m)} f_{(m+1)}. \tag{3.15}$$

The time derivatives at a grid point j in the pth stage of Runge–Kutta time integration are defined as

$$k_j^{n,p} = \varphi_0 f^{n,p}(x_j) + \varphi_1 f_x^{n,p}(x_j) + \varphi_2 f_{xx}^{n,p}(x_j) + \cdots + \varphi_{(m)} f_{(m)}^{n,p}(x_j), \tag{3.16}$$

$$k_{x,j}^{n,p} = \varphi_0 f_x^{n,p}(x_j) + \varphi_1 f_{xx}^{n,p}(x_j) + \varphi_2 f_{xxx}^{n,p}(x_j) + \cdots + \varphi_{(m)} f_{(m+1)}^{n,p}(x_j), \tag{3.17}$$

where the notation n is the time step index. We assume the spatial profiles of the time derivatives to be

$$k_j^{n,p} = \sum_k \hat{f}_t^{n,p}(k) \mathrm{e}^{\mathrm{i}wx_j/h}, \tag{3.18}$$

and

$$k_{x,j}^{n,p} = \sum_k \hat{f}_{tx}^{n,p}(k) \mathrm{e}^{\mathrm{i}wx_j/h}. \tag{3.19}$$

Substituting Eqs. (3.18) and (3.19) into Eqs. (3.16) and (3.17) and using the derivative approximations (3.7), we have

$$\begin{aligned}\hat{f}_t^{n,p}(k) &= (\varphi_0 + \varphi_2 A_{(2)}(w) + \varphi_3 A_{(3)}(w) + \cdots + \varphi_m A_{(m)}(w))\hat{f}^{n,p}(k) \\ &\quad + (\varphi_1 + \varphi_2 A'_{(2)}(w) + \varphi_3 A'_{(3)}(w) + \cdots + \varphi_m A'_{(m)}(w))\hat{f}_x^{n,p}(k), \end{aligned} \tag{3.20}$$

$$\begin{aligned}\hat{f}_{tx}^{n,p}(k) &= (\varphi_1 A_{(2)}(w) + \varphi_2 A_{(3)}(w) + \cdots + \varphi_m A_{(m+1)}(w))\hat{f}^{n,p}(k) \\ &\quad + (\varphi_0 + \varphi_1 A'_2(w) + \varphi_2 A'_3(w) + \cdots + \varphi_m A'_{(m+1)}(w))\hat{f}_x^{n,p}(k). \end{aligned} \tag{3.21}$$

Eqs. (3.20) and (3.21) are rewritten by the matrix form of

$$\mathbf{D}_{n,p} = \mathbf{A}\mathbf{F}_{n,p}, \tag{3.22}$$

where

$$\mathbf{D}_{n,p} = \begin{pmatrix} \hat{f}_t^{n,p}(k) \\ \hat{f}_{tx}^{n,p}(k) \end{pmatrix}, \tag{3.23}$$

$$\mathbf{A} = \begin{pmatrix} \varphi_0 + \sum_{m=2}^{m} \varphi_m A_{(m)}(w) & \varphi_1 + \sum_{m=2}^{m} \varphi_m A'_{(m)}(w) \\ \sum_{m=1}^{m} \varphi_m A_{(m+1)}(w) & \varphi_0 + \sum_{m=1}^{m} \varphi_m A'_{(m+1)}(w) \end{pmatrix} = \begin{pmatrix} A_{11}(w) & A_{12}(w) \\ A_{21}(w) & A_{22}(w) \end{pmatrix}, \tag{3.24}$$

$$\mathbf{F}_{n,p} = \begin{pmatrix} \hat{f}^{n,p}(k) \\ \hat{f}_x^{n,p}(k) \end{pmatrix}. \tag{3.25}$$

Eqs. (2.13) and (2.14) lead to

$$\mathbf{F}_{n,p} = \mathbf{F}_n + \Delta t \sum_q \alpha_{pq} \mathbf{D}_{n,q}, \tag{3.26}$$

where

$$\mathbf{F}_n = \begin{pmatrix} \hat{f}^n(k) \\ \hat{f}_x^n(k) \end{pmatrix}. \tag{3.27}$$

Substituting Eq. (3.26) into Eq. (3.22), we have

$$\mathbf{P}\mathbf{Q} = \mathbf{R}, \tag{3.28}$$

where

$$\mathbf{P} = \begin{pmatrix} \mathbf{P}_{11} & \mathbf{P}_{12} & \cdot & \cdot & \mathbf{P}_{1p} \\ \mathbf{P}_{21} & \mathbf{P}_{22} & \cdot & \cdot & \cdot \\ \cdot & \cdot & \cdot & \cdot & \cdot \\ \cdot & \cdot & \cdot & \mathbf{P}_{p-1p-1} & \mathbf{P}_{p-1p} \\ \mathbf{P}_{p1} & \cdot & \cdot & \mathbf{P}_{pp-1} & \mathbf{P}_{pp} \end{pmatrix}, \quad \mathbf{P}_{pq} = \begin{cases} 1 - \Delta t \alpha_{pq} \mathbf{A} & (p = q), \\ -\Delta t \alpha_{pq} \mathbf{A} & (p \neq q), \end{cases} \tag{3.29}$$

$$\mathbf{Q} = \begin{pmatrix} \mathbf{D}_{n,1} \\ \mathbf{D}_{n,2} \\ \cdot \\ \cdot \\ \mathbf{D}_{n,p} \end{pmatrix}, \tag{3.30}$$

$$\mathbf{R} = \begin{pmatrix} \mathbf{AF}_n \\ \mathbf{AF}_n \\ \cdot \\ \cdot \\ \mathbf{AF}_n \end{pmatrix}. \tag{3.31}$$

From $\mathbf{P}^{-1}\mathbf{PQ} = \mathbf{Q} = \mathbf{P}^{-1}\mathbf{R}$, the Fourier coefficients of time derivatives can be written as the function of the physical variables and the first-order derivatives at nth time step:

$$\mathbf{D}_{n,p} = \mathbf{B}_p \mathbf{AF}_n, \tag{3.32}$$

where

$$\mathbf{B}_p = \sum_q \mathbf{C}_{pq}, \tag{3.33}$$

and $\mathbf{C}_{pq}$ is the component of the set (p, q) in the matrix $\mathbf{P}^{-1}$. Eqs. (2.15) and (2.16) lead to

$$\mathbf{F}_{n+1} = \mathbf{F}_n + \Delta t \sum_p \beta_p \mathbf{D}_{n,p}. \tag{3.34}$$

From Eqs. (3.32) and (3.34), the Runge–Kutta time integration of the IDO scheme are derived:

$$\mathbf{F}_{n+1} = \mathbf{SF}_n, \tag{3.35}$$

where

$$\mathbf{S} = \mathbf{I} + \Delta t \mathbf{A} \sum_p \beta_p \mathbf{B}_p = \begin{pmatrix} S_{11}(w) & S_{12}(w) \\ S_{21}(w) & S_{22}(w) \end{pmatrix}. \tag{3.36}$$

The matrix $\mathbf{S}$ is determined as follows:

For the one-stage method:

$$S_{11} = 1 + \overline{A}_{11}, \quad S_{12} = \overline{A}_{12}, \quad S_{21} = \overline{A}_{21}, \quad S_{22} = 1 + \overline{A}_{22}. \tag{3.37}$$

For the two-stage method:

$$\begin{aligned} S_{11} &= 1 + \overline{A}_{11} + \frac{\overline{A}_{11}^2}{2} + \frac{\overline{A}_{12}\overline{A}_{21}}{2}, \quad S_{12} = \overline{A}_{12} + \frac{\overline{A}_{11}\overline{A}_{12}}{2} + \frac{\overline{A}_{12}\overline{A}_{22}}{2}, \\ S_{21} &= \overline{A}_{21} + \frac{\overline{A}_{11}\overline{A}_{21}}{2} + \frac{\overline{A}_{21}\overline{A}_{22}}{2}, \quad S_{22} = 1 + \overline{A}_{22} + \frac{\overline{A}_{22}^2}{2} + \frac{\overline{A}_{12}\overline{A}_{21}}{2}. \end{aligned} \tag{3.38}$$

For the three-stage method:

$$\begin{aligned} S_{11} &= 1 + \overline{A}_{11} + \frac{\overline{A}_{11}^2}{2} + \frac{\overline{A}_{11}^3}{6} + \frac{\overline{A}_{12}\overline{A}_{21}}{2} + \frac{\overline{A}_{11}\overline{A}_{12}\overline{A}_{21}}{3} + \frac{\overline{A}_{12}\overline{A}_{21}\overline{A}_{22}}{6}, \\ S_{12} &= \overline{A}_{12} + \frac{\overline{A}_{11}\overline{A}_{12}}{2} + \frac{\overline{A}_{11}^2\overline{A}_{12}}{6} + \frac{\overline{A}_{11}\overline{A}_{12}\overline{A}_{22}}{6} + \frac{\overline{A}_{12}\overline{A}_{22}}{2} + \frac{\overline{A}_{12}\overline{A}_{22}^2}{6} + \frac{\overline{A}_{12}^2\overline{A}_{21}}{6}, \\ S_{21} &= \overline{A}_{21} + \frac{\overline{A}_{21}\overline{A}_{22}}{2} + \frac{\overline{A}_{21}\overline{A}_{22}^2}{6} + \frac{\overline{A}_{11}\overline{A}_{21}\overline{A}_{22}}{6} + \frac{\overline{A}_{11}\overline{A}_{21}}{2} + \frac{\overline{A}_{11}^2\overline{A}_{21}}{6} + \frac{\overline{A}_{12}\overline{A}_{21}^2}{6}, \\ S_{22} &= 1 + \overline{A}_{22} + \frac{\overline{A}_{22}^2}{2} + \frac{\overline{A}_{22}^3}{6} + \frac{\overline{A}_{12}\overline{A}_{21}}{2} + \frac{\overline{A}_{12}\overline{A}_{21}\overline{A}_{22}}{3} + \frac{\overline{A}_{11}\overline{A}_{12}\overline{A}_{21}}{6}. \end{aligned} \tag{3.39}$$

For the four-stage method:

$$
\begin{aligned}
S_{11} &= 1+\overline{A}_{11}+\frac{\overline{A}_{11}^2}{2}+\frac{\overline{A}_{11}^3}{6}+\frac{\overline{A}_{11}^4}{24}+\frac{\overline{A}_{12}\overline{A}_{21}}{2}+\frac{\overline{A}_{11}\overline{A}_{12}\overline{A}_{21}}{3}+\frac{\overline{A}_{11}^2\overline{A}_{12}\overline{A}_{21}}{8}\\
&\quad+\frac{\overline{A}_{12}\overline{A}_{21}\overline{A}_{22}}{6}+\frac{\overline{A}_{12}\overline{A}_{21}\overline{A}_{22}^2}{24}+\frac{\overline{A}_{11}\overline{A}_{12}\overline{A}_{21}\overline{A}_{22}}{12}+\frac{\overline{A}_{12}^2\overline{A}_{21}^2}{24},\\
S_{12} &= \overline{A}_{12}+\frac{\overline{A}_{11}\overline{A}_{12}}{2}+\frac{\overline{A}_{11}^2\overline{A}_{12}}{6}+\frac{\overline{A}_{11}^3\overline{A}_{12}}{24}+\frac{\overline{A}_{11}\overline{A}_{12}\overline{A}_{22}}{6}+\frac{\overline{A}_{11}^2\overline{A}_{12}\overline{A}_{22}}{24}+\frac{\overline{A}_{11}\overline{A}_{12}\overline{A}_{22}^2}{24}+\frac{\overline{A}_{11}\overline{A}_{12}^2\overline{A}_{21}}{12}\\
&\quad+\frac{\overline{A}_{12}\overline{A}_{22}}{2}+\frac{\overline{A}_{12}\overline{A}_{22}^2}{6}+\frac{\overline{A}_{12}\overline{A}_{22}^3}{24}+\frac{\overline{A}_{12}^2\overline{A}_{21}}{6}+\frac{\overline{A}_{12}^2\overline{A}_{21}\overline{A}_{22}}{12},\\
S_{21} &= \overline{A}_{21}+\frac{\overline{A}_{21}\overline{A}_{22}}{2}+\frac{\overline{A}_{21}\overline{A}_{22}^2}{6}+\frac{\overline{A}_{21}\overline{A}_{22}^3}{24}+\frac{\overline{A}_{11}\overline{A}_{21}\overline{A}_{22}}{6}+\frac{\overline{A}_{11}\overline{A}_{21}\overline{A}_{22}^2}{24}\\
&\quad+\frac{\overline{A}_{11}^2\overline{A}_{21}\overline{A}_{22}}{24}+\frac{\overline{A}_{12}\overline{A}_{21}^2\overline{A}_{22}}{12}+\frac{\overline{A}_{11}\overline{A}_{21}}{2}+\frac{\overline{A}_{11}^2\overline{A}_{21}}{6}+\frac{\overline{A}_{11}^3\overline{A}_{21}}{24}+\frac{\overline{A}_{12}\overline{A}_{21}^2}{6}+\frac{\overline{A}_{11}\overline{A}_{12}\overline{A}_{21}^2}{12},\\
S_{22} &= 1+\overline{A}_{22}+\frac{\overline{A}_{22}^2}{2}+\frac{\overline{A}_{22}^3}{6}+\frac{\overline{A}_{22}^4}{24}+\frac{\overline{A}_{12}\overline{A}_{21}}{2}+\frac{\overline{A}_{12}\overline{A}_{21}\overline{A}_{22}}{3}+\frac{\overline{A}_{12}\overline{A}_{21}\overline{A}_{22}^2}{8}+\frac{\overline{A}_{11}\overline{A}_{12}\overline{A}_{21}}{6}\\
&\quad+\frac{\overline{A}_{11}^2\overline{A}_{12}\overline{A}_{21}}{24}+\frac{\overline{A}_{11}\overline{A}_{12}\overline{A}_{21}\overline{A}_{22}}{12}+\frac{\overline{A}_{12}^2\overline{A}_{21}^2}{24},
\end{aligned}
\tag{3.40}
$$

where $\overline{A}_{ij}$ is $A_{ij}\Delta t$. We obtain the matrix at nth time step from Eq. (3.35) as

$$
\mathbf{F}_n = \mathbf{S}\mathbf{F}_{n-1} = \mathbf{S}^2\mathbf{F}_{n-2} = \cdots = \mathbf{S}^n\mathbf{F}_0. \tag{3.41}
$$

Eigenvalues and eigenvectors for the coefficient matrix $\mathbf{S}$ are defined as $\lambda^{\pm}$ and $\mathbf{K}^{\pm}$. Using $\lambda^{\pm}$ and $\mathbf{K}^{\pm}$, we have

$$
\mathbf{F}_n = \mathbf{L}\begin{pmatrix}\lambda^+ & 0\\ 0 & \lambda^-\end{pmatrix}^n\mathbf{L}^{-1}\mathbf{F}_0, \tag{3.42}
$$

where $\mathbf{L} = (\mathbf{K}^+\mathbf{K}^-)$ and $\mathbf{L}\mathbf{L}^{-1} = \mathbf{I}$.

4. Accuracy for advection equation

The one-dimensional advection equation with a negative constant velocity is considered:

$$
\frac{\partial f}{\partial t} = -u\frac{\partial f}{\partial x}. \tag{4.1}
$$

Eq. (4.1) is obtained substituting $\varphi_1 = -u$ and the other coefficients $\varphi_{(m)} = 0$ into Eq. (3.14). The IDO scheme solves the additional equation,

$$
\frac{\partial^2 f}{\partial t\partial x} = -u\frac{\partial^2 f}{\partial x^2}, \tag{4.2}
$$

for the time integration of first-order derivatives.

4.1. The fifth-order central IDO scheme

The coefficient matrix $\mathbf{A}$ (3.24) of the IDO scheme with the fifth-order central interpolation function (2.1) (the fifth-order central IDO scheme) is given by

$$
\begin{pmatrix}A_{11} & A_{12}\\ A_{21} & A_{22}\end{pmatrix} = \begin{pmatrix}0 & -u\\ -uA_{(2)} & -uA'_{(2)}\end{pmatrix} = \begin{pmatrix}0 & \frac{Ch}{\Delta t}\\ \frac{4C}{h\Delta t}(\cos w-1) & -\mathrm{i}\frac{C}{\Delta t}\sin w\end{pmatrix}, \tag{4.3}
$$

where $C = |u|\Delta t/h$ denotes the Courant number and Eq. (3.8) is used.

In order to obtain stable time integration, the absolute values of both the eigenvalues $|\lambda^{\pm}|$ in Eq. (3.42) should be less than unity for all the wavenumbers and the given Courant number. The contour plots of the

eigenvalue $|\lambda| = \max(|\lambda^+|, |\lambda^-|)$ for the first-order time integration are shown in Fig. 1(a). The horizontal axis means the wavenumber and the vertical axis is the Courant number. For almost all the Courant numbers, the eigenvalues are larger than unity. The first-order explicit time integration of the IDO scheme is found to be unstable. The eigenvalues for the two-, the three-, and the four-stage Runge–Kutta time integration are illustrated in Fig. 1(b)–(d). The two-stage Runge–Kutta method still has a large unstable area. By using the three-stage or the four-stage method, we can greatly enlarge the stable area for the advection calculation. The stable Courant number for the three-stage method is estimated to be $C < 0.55$, and that of the four-stage method is $C < 0.94$.

In order to estimate dispersion error and dissipation error for the solution, we define an amplification factor at nth time step to the initial time step:

$$g_n(w) = |g_n(w)|e^{i\alpha_n(w)} = \frac{\hat{f}^n(k)}{\hat{f}^0(k)}, \tag{4.4}$$

where $|g_n|$ and α_n represent gain and phase, respectively. The exact solution of the gain are unity, and the exact phase is $\alpha_n = Cwn$.

We examine the phase for various central schemes, which include the IDO scheme, the second-, the fourth-, and the sixth-order central FD schemes, the fourth-order CD scheme, and the sixth-order Combined CD (CCD) scheme [17], with the four-stage Runge–Kutta time integration. Only for the initial time step,

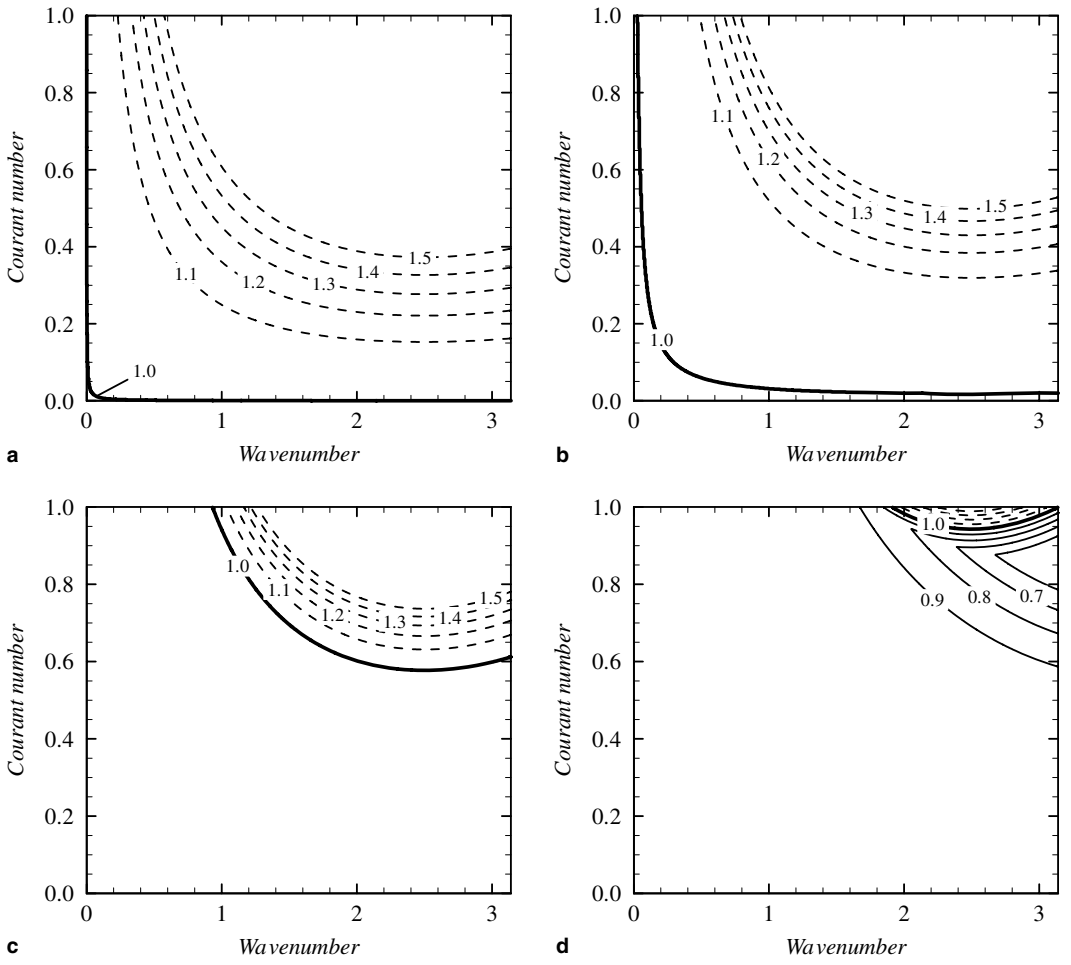

Fig. 1. Contour plots of eigenvalues of the fifth-order central IDO scheme for the advection equation: (a) first-order explicit time integration; (b) two-stage Runge–Kutta method; (c) three-stage Runge–Kutta method; (d) four-stage Runge–Kutta method.

the relation of $\hat{f}_x^0(k) = \mathrm{i}w/h\hat{f}^0(k)$ is used for the IDO scheme. Fig. 2(a), (b), and (c) show the phases for $Cn = 100$ with the Courant numbers 0.1, 0.2, and 0.4, respectively. When we use $N = 100$ grid points, the initial profile propagates from $x = x_j$ to $x = x_j + L$ for $Cn = 100$. In these figures, the phases are normalized as $\bar{\alpha} = \alpha_n/Cn$. Significant differences could not be seen between these Courant numbers. The phases for the fifth-order central IDO scheme follow the exact solution more closely than the other schemes for a wide range of the wavenumber. The phase error, defined by

$$P_{\mathrm{E}} = \left|\frac{w - \bar{\alpha}}{w}\right|, \tag{4.5}$$

for the Courant number 0.1 is plotted in Fig. 3. The phase error for the IDO scheme has fourth-order convergence for the wavenumber. It should be noted that the IDO scheme can resolve high wavenumbers more accurately than the CCD scheme. The range of the resolved wavenumber with $P_{\mathrm{E}} < 1\%$ is estimated as $w < 1.86$ for the IDO scheme, and that of the CCD scheme is $w < 1.80$. From Fig. 4, the gains for these central schemes are unity for all the wavenumbers. The central IDO scheme provides less-dispersive and non-dissipative solution for all the wavenumbers, and we can therefore obtain spectral-like results for DNS of turbulence [16]. For wavenumbers near $w = \pi$, the phase error becomes non-negligible even in the IDO scheme, and this causes non-physical oscillations. The central schemes need the presence of physical viscosity or additional numerical viscosity for stable computation of the flow including such wavenumbers.

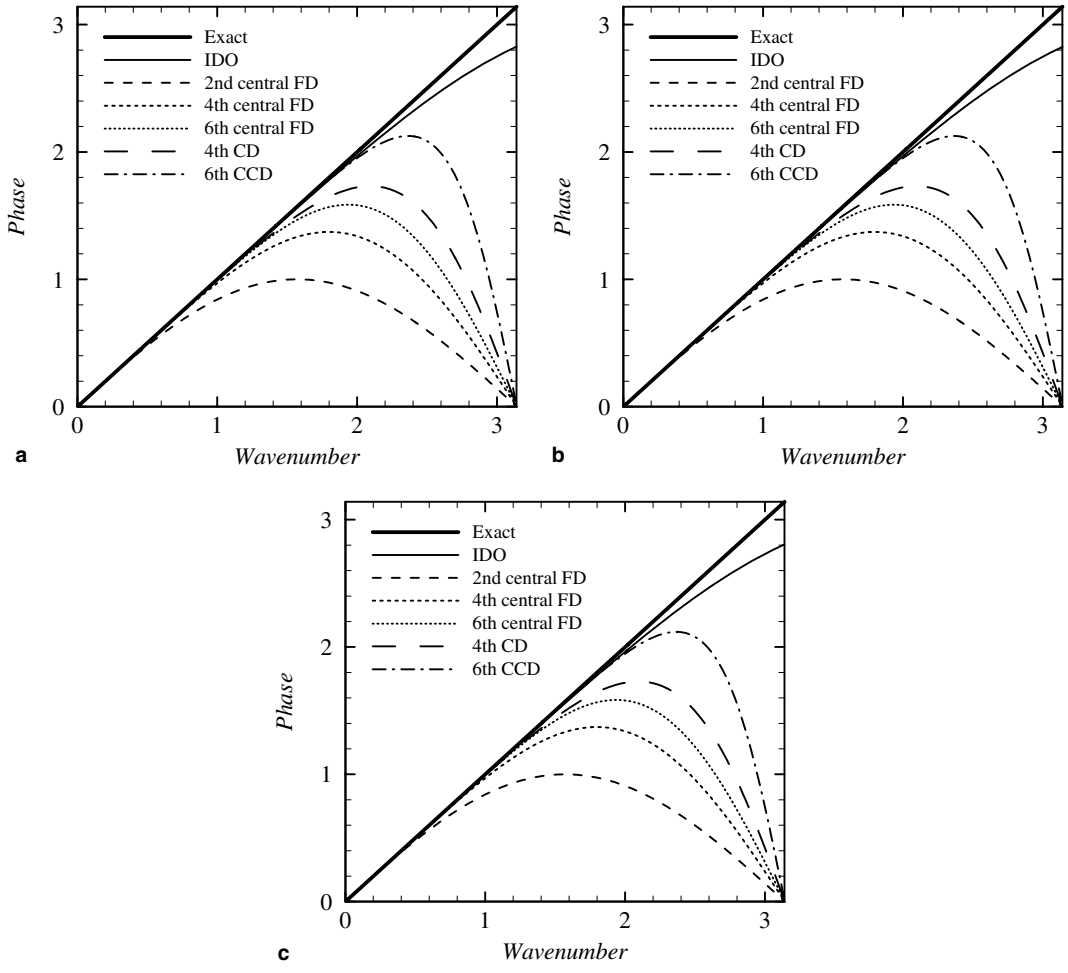

Fig. 2. Phases for the central schemes with the Courant number of (a) 0.1, (b) 0.2, and (c) 0.4. The phases are normalized as $\bar{\alpha} = \alpha_n/Cn$.

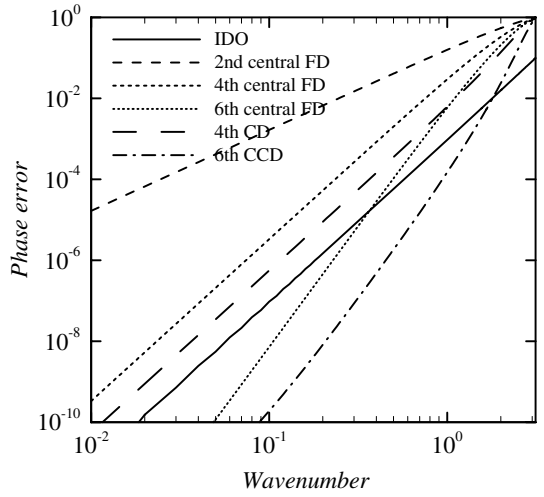

Fig. 3. Phase errors for the central schemes with the Courant number 0.1.

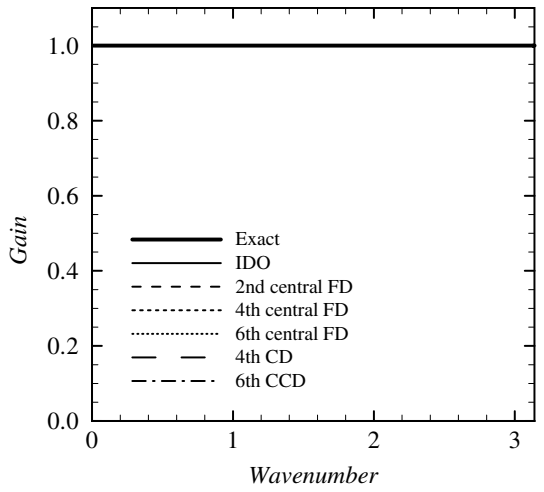

Fig. 4. Gains for the central schemes. All the lines are overwritten by the exact gain.

4.2. The third-order upwind IDO scheme

Since the advection equation has only one characteristics of PDE, the upwind interpolation function (2.6) can be applied. The coefficient matrix **A** (3.24) for the IDO scheme with the upwind interpolation function (the third-order upwind IDO scheme) are described as

$$\begin{pmatrix} A_{11} & A_{12} \\ A_{21} & A_{22} \end{pmatrix} = \begin{pmatrix} 0 & \frac{Ch}{\Delta t} \\ \frac{6C}{h\Delta t}(e^{iw}-1) & -\frac{2C}{\Delta t}(e^{iw}+2) \end{pmatrix}, \tag{4.6}$$

where Eq. (3.12) is used.

The eigenvalues of the third-order upwind IDO scheme for the first-order explicit time integration and for the two-, the three-, and the four-stage Runge–Kutta time integration are illustrated in Fig. 5. The increased stability deriving from the higher-order Runge–Kutta method can be confirmed. The solution with the four-stage Runge–Kutta method is found to be stable for the Courant number $C < 0.46$.

The phases $\bar{\alpha} = \alpha_n/Cn$ for the third-order upwind IDO scheme with the Courant numbers 0.1, 0.2, and 0.4 are shown in Fig. 6. As references, the phases for the first-, and the third-order upwind FD schemes, for the CIP scheme, and for the Cubic Lagrange (CUL) scheme are shown. The four-stage Runge–Kutta

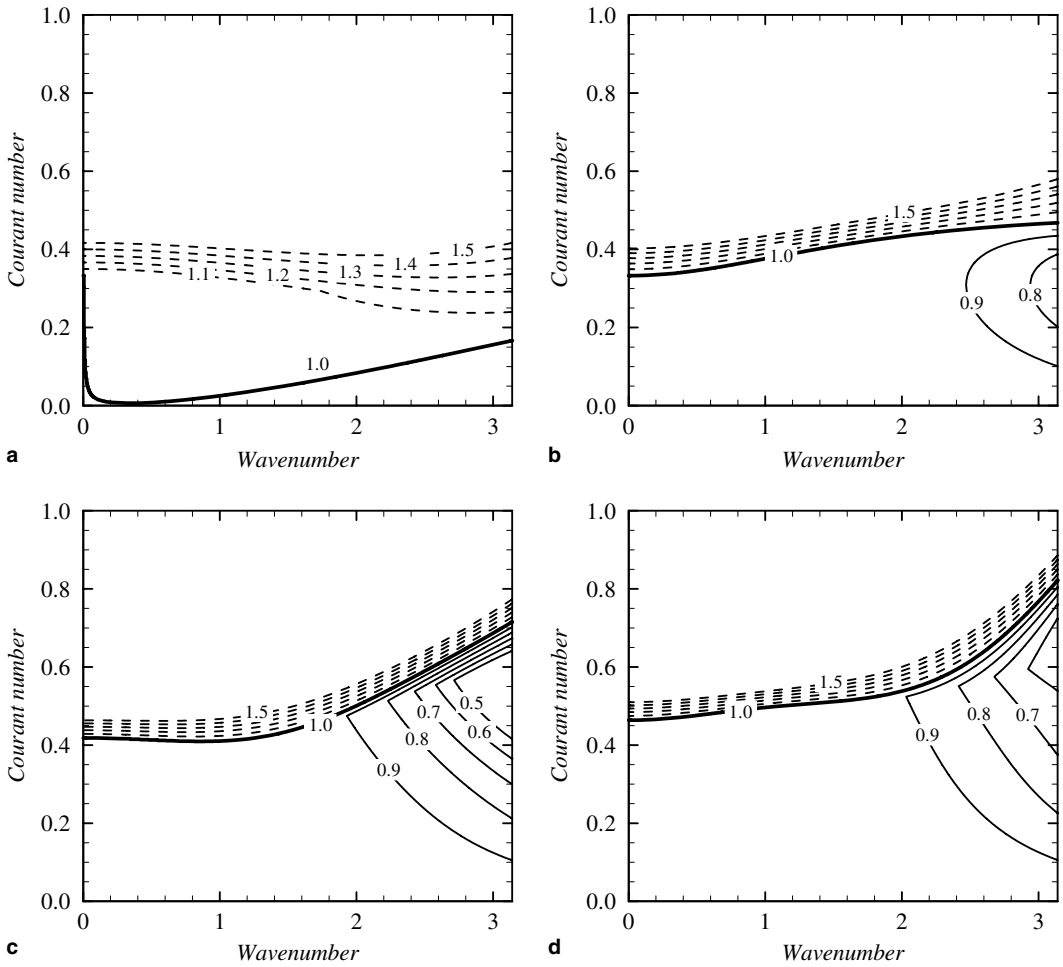

Fig. 5. Contour plots of eigenvalues of the third-order upwind IDO scheme for the advection equation: (a) first-order explicit time integration; (b) two-stage Runge–Kutta method; (c) three-stage Runge–Kutta method; (d) four-stage Runge–Kutta method.

method is used for the time integration of the IDO scheme and the FD schemes. The upwind IDO scheme and the CIP scheme can resolve higher wavenumbers than the upwind FD schemes and the CUL scheme. Fig. 6 also presents the phase for the seventh-order upwind IDO scheme, where the seventh-order interpolation function, covering the domain from grid point $j-1$ to $j+2$, is adopted. The seventh-order IDO scheme provides the approximately equal phase to the exact one for all the wavenumbers. Fig. 7 gives the phase error estimated by Eq. (4.5). The third-order IDO scheme has fourth-order accuracy and the seventh-order IDO scheme has 6.5th order. The third-order upwind IDO scheme resolves a wavenumber of $w < 1.43$ with an error of $P_E < 1\%$. Note that even for $w = \pi$, the error for the seventh-order IDO scheme is estimated as 0.88%.

Fig. 8 presents the normalized gains, $\bar{g} = |g_n|^{\frac{1}{Cn}}$, for these schemes with the Courant numbers 0.1, 0.2 and 0.4. The gains of the upwind schemes are less than unity for the entire region of the wavenumber. Since the gains of the upwind IDO scheme and the CIP scheme are closer to unity than the other upwind schemes, less dissipative solutions are achieved by using these schemes. The gain error,

$$G_E = |1 - \bar{g}^{\frac{1}{w}}|, \tag{4.7}$$

is given in Fig. 9, where the Courant number is 0.1. According to the figure, the gain error for the CIP scheme and the third-order upwind IDO scheme are of fourth-order, and that of the seventh-order IDO scheme is 6.4th order.

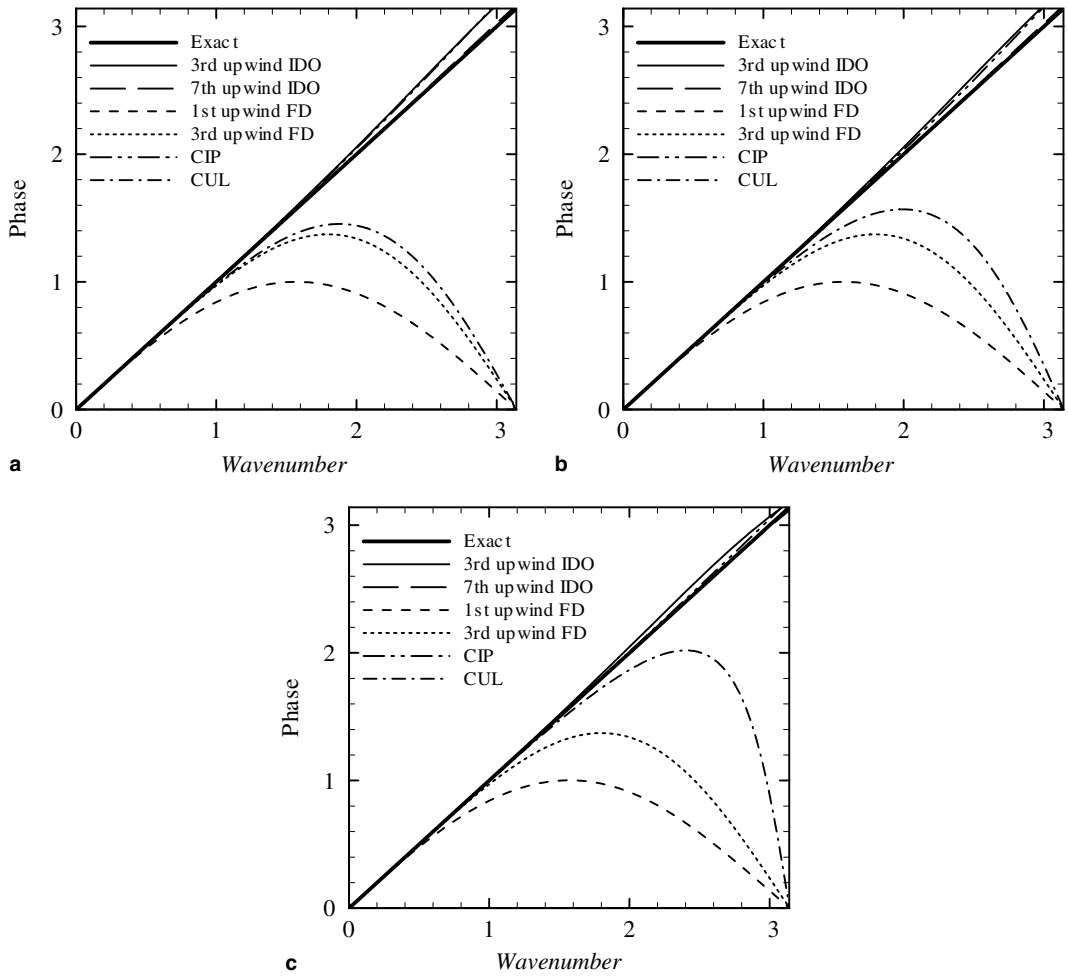

Fig. 6. Phases for the upwind schemes with the Courant number of (a) 0.1, (b) 0.2, and (c) 0.4.

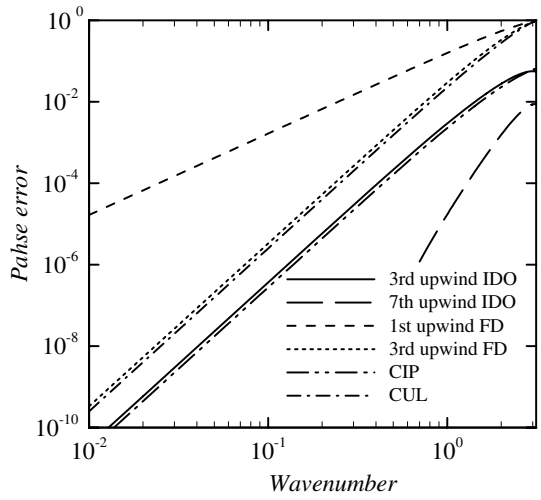

Fig. 7. Phase errors for the upwind schemes with the Courant number 0.1.

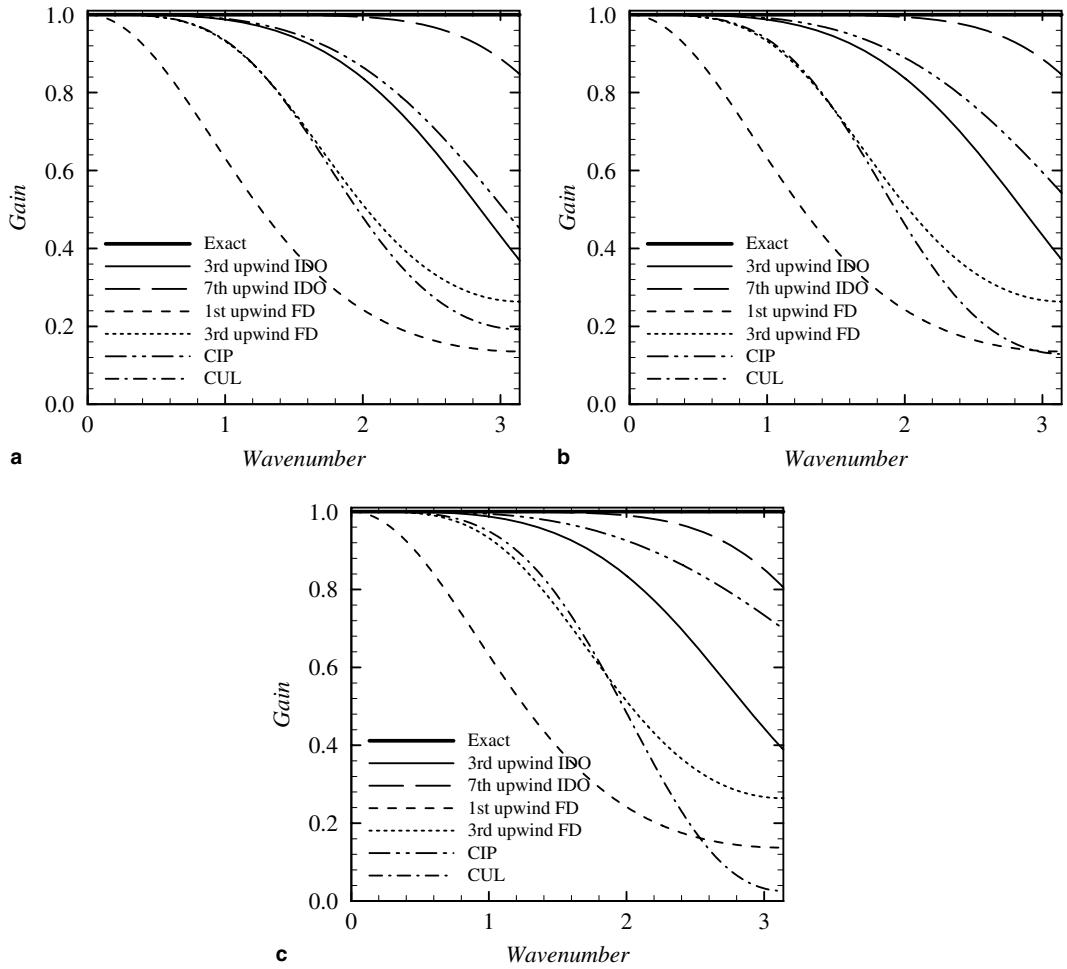

Fig. 8. Gain curves for the upwind schemes with the Courant number of (a) 0.1, (b) 0.2, and (c) 0.4. The gains are normalized as $\bar{g} = |g_n|^{\frac{1}{Cn}}$.

4.3. Numerical viscosity in the upwind IDO scheme

It is well known that the first-order upwind FD consists of the first- and the second-order derivatives of the second-order central FD. The derivatives (2.7) and (2.8) of the third-order upwind interpolation function can be expressed by the derivatives (2.2)–(2.5) of the fifth-order central interpolation function. The second-order derivative (2.7) is assumed to be

$$f_{xx}^{\text{upwind}}(x_j) = \sum_{m=0}^{5} v_{(m)} f_{(m)}^{\text{central}}(x_j). \tag{4.8}$$

Substituting the physical variable and the derivatives of each interpolation function into f_{xx}^{upwind} and $f_{(m)}^{\text{central}}$, we have

$$\begin{pmatrix} 0 & 0 & 2/h^2 & 15/2h^3 & -12/h^4 & -90/h^5 \\ 1 & 0 & -4/h^2 & 0 & 24/h^4 & 0 \\ 0 & 0 & 2/h^2 & -15/2h^3 & -12/h^4 & 90/h^5 \\ 0 & 0 & -1/2h & -3/2h^2 & 6/h^3 & 30/h^4 \\ 0 & 1 & 0 & -12/h^2 & 0 & 120/h^4 \\ 0 & 0 & 1/2h & -3/2h^2 & -6/h^3 & 30/h^4 \end{pmatrix} \begin{pmatrix} v_0 \\ v_1 \\ v_2 \\ v_3 \\ v_4 \\ v_5 \end{pmatrix} = \begin{pmatrix} 6\omega/h'^2 \\ -6/h'^2 \\ 6(1-\omega)/h'^2 \\ -2\omega/h' \\ -4/h' \\ -2(1-\omega)/h' \end{pmatrix}, \tag{4.9}$$

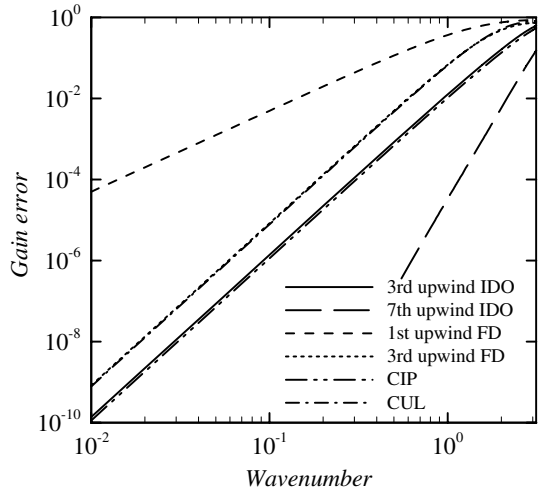

Fig. 9. Gain errors for the upwind schemes with the Courant number 0.1.

where $\omega = 1$ as $u < 0$, and $\omega = 0$ as $u > 0$. Using $h' = h$ as $u < 0$ and $h' = -h$ as $u > 0$, the coefficients are derived to

$$\begin{pmatrix} v_0 \\ v_1 \\ v_2 \\ v_3 \\ v_4 \\ v_5 \end{pmatrix} = \begin{pmatrix} 0 \\ 0 \\ 1 \\ 0 \\ -h'^2/12 \\ -h'^3/30 \end{pmatrix}. \tag{4.10}$$

Similarly, the third-order derivative (2.8) is expressed as

$$f_{xxx}^{\text{upwind}}(x_j) = \sum_{m=0}^{5} \kappa_{(m)} f_{(m)}^{\text{central}}(x_j), \tag{4.11}$$

$$\begin{pmatrix} \kappa_0 \\ \kappa_1 \\ \kappa_2 \\ \kappa_3 \\ \kappa_4 \\ \kappa_5 \end{pmatrix} = \begin{pmatrix} 0 \\ 0 \\ 0 \\ 1 \\ h'/2 \\ 3h'^2/20 \end{pmatrix}. \tag{4.12}$$

From these expressions, it is found that the upwind interpolation function (2.6) includes the numerical viscosity terms of the fourth- and the fifth-order derivatives. The numerical viscosity contributes to stabilize the solution for high wavenumbers. We can improve the CIP scheme and the upwind IDO scheme by adjusting the coefficients v and κ.

As an example, the phase and the gain for an improved IDO scheme with the Courant number 0.2 are described in Fig. 10, where the coefficients of $v_0 = v_1 = v_3 = 0$, $v_2 = 1$, $v_4 = -h'^2/40$, $v_5 = -h'^3/60$ are used. The phase plots show that the improved scheme has better resolution than the fifth-order central and the third-order upwind IDO schemes. The range of the wavenumber with $P_E < 1\%$ is enlarged to $w < 2.53$ by using these coefficients. The gain of the improved scheme is closer to the exact gain than that of the third-order upwind IDO scheme. The optimization of the coefficients will be discussed in the next paper.

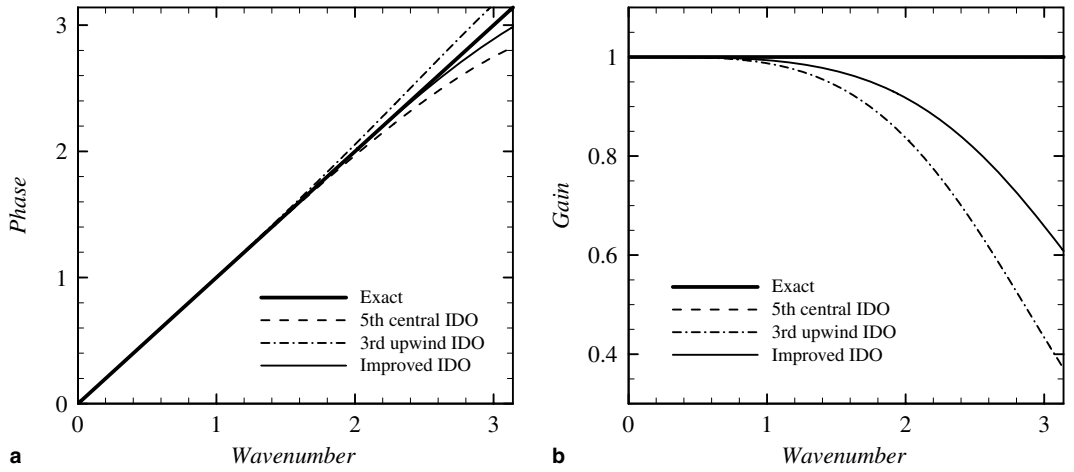

Fig. 10. Results for the improved IDO scheme: (a) phase; (b) gain. The gain for the fifth-order central IDO scheme is overwritten by the exact gain.

5. Accuracy for diffusion equation

The one-dimensional diffusion equation,

$$\frac{\partial f}{\partial t} = \kappa \frac{\partial^2 f}{\partial x^2}, \tag{5.1}$$

corresponds to Eq. (3.14) with $\varphi_2 = \kappa$ and the other coefficients $\varphi_m = 0$. The differentiated equation of Eq. (5.1) is also solved:

$$\frac{\partial^2 f}{\partial t \partial x} = \kappa \frac{\partial^3 f}{\partial x^3}. \tag{5.2}$$

By using the fifth-order central IDO scheme, the coefficient matrix **A** (3.24) for the diffusion equation is defined as

$$\begin{pmatrix} A_{11} & A_{12} \\ A_{21} & A_{22} \end{pmatrix} = \begin{pmatrix} \kappa A_{(2)} & \kappa A'_{(2)} \\ \kappa A_{(3)} & \kappa A'_{(3)} \end{pmatrix} = \begin{pmatrix} \frac{4\mu}{\Delta t}(\cos w - 1) & -\mathrm{i}\frac{\mu h}{\Delta t}\sin w \\ \mathrm{i}\frac{15\mu}{h\Delta t}\sin w & -\frac{3\mu}{\Delta t}(\cos w + 4) \end{pmatrix}, \tag{5.3}$$

where $\mu = \kappa \Delta t / h^2$ represents the diffusion number and Eqs. (3.8) and (3.9) are applied. The eigenvalues of the matrix **S** (3.36) for the first-order explicit time integration, and for the two-, the three-, the four-stage Runge–Kutta methods are illustrated in Fig. 11(a)–(d). The three- or the four-stage Runge–Kutta time integration extends the range of the stable diffusion number in a similar way with the advection equation. The calculations are stable up to $\mu = 0.13$ for the two-stage Runge–Kutta method, $\mu = 0.16$ for the three-stage method, and $\mu = 0.18$ for the four-stage method. Implicit time integration makes the computation of the IDO scheme stable comparably to FD schemes. Fig. 11(e) describes the eigenvalues for the first-order implicit time integration. The eigenvalues are confirmed to be less than unity for the whole area.

The accuracy of the IDO scheme is compared to that of FD and CD schemes. For the amplification factor (4.4) of the diffusion equation, the exact gain is given as follows:

$$|g_n(w)| = \mathrm{e}^{-\mu w^2 n}. \tag{5.4}$$

The exact phase and the numerical phase for the central schemes are zero. The numerical error for the diffusion equation is defined as

$$E(w) = \left| |g_n^{\text{exact}}|^{\frac{1}{\mu w^2 n}} - |g_n^{\text{numerical}}|^{\frac{1}{\mu w^2 n}} \right|. \tag{5.5}$$

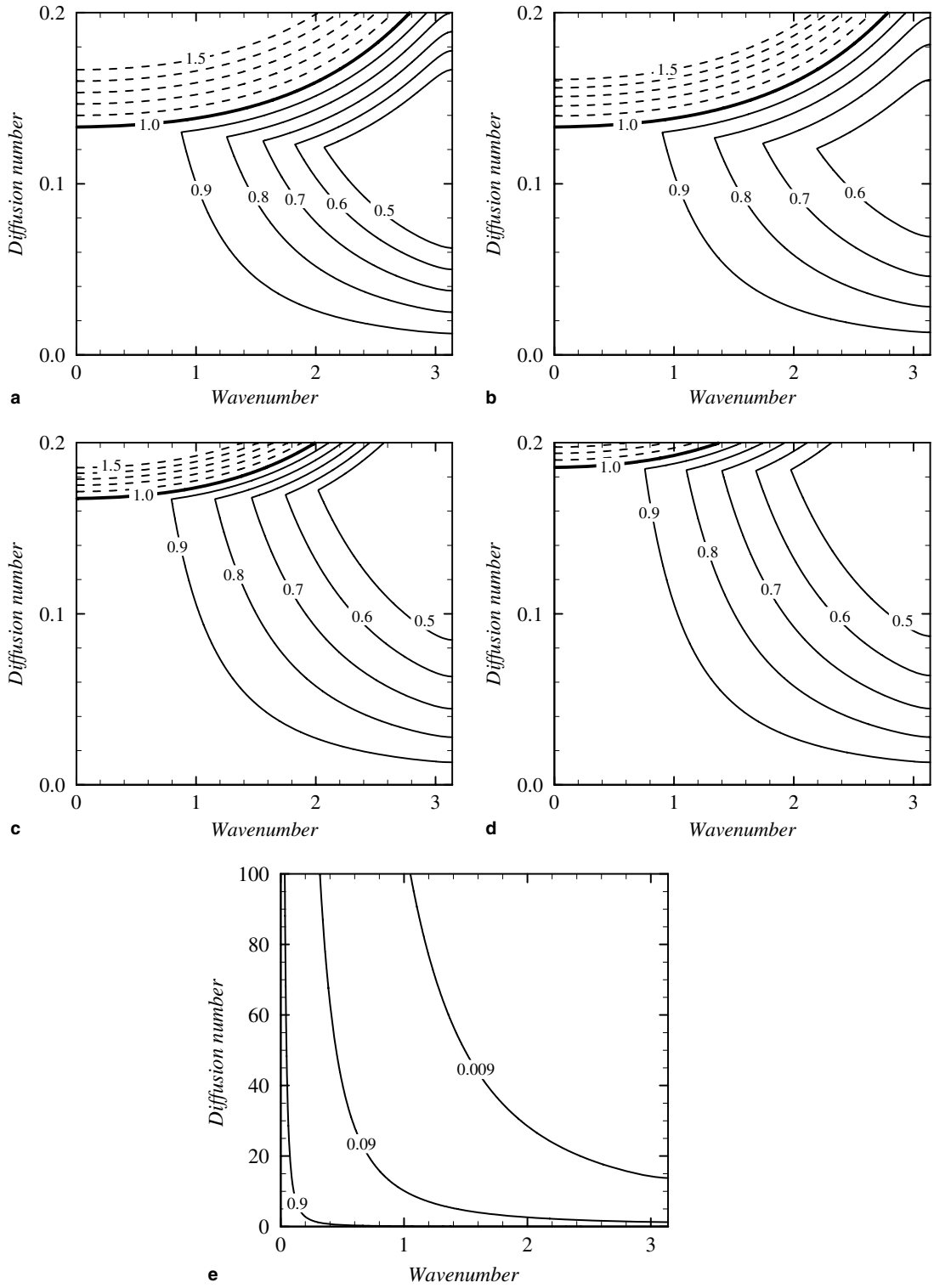

Fig. 11. Contour plots of eigenvalues of the fifth-order central IDO scheme for the diffusion equation: (a) first-order explicit time integration; (b) two-stage Runge–Kutta method; (c) three-stage Runge–Kutta method; (d) four-stage Runge–Kutta method; (e) first-order implicit time integration.

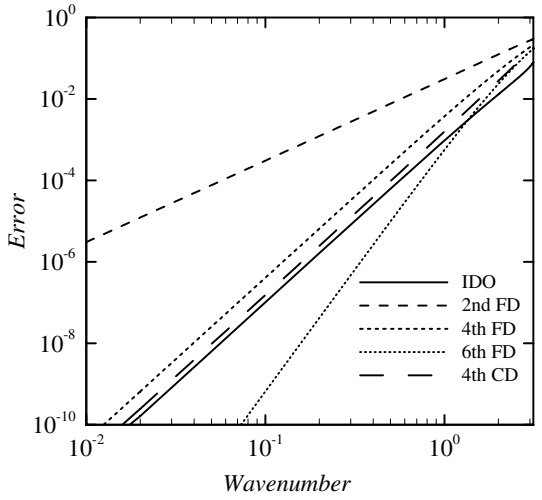

Fig. 12. Error plots for the diffusion equation.

The errors for $n = 10$ and $\mu = 0.1$ are shown in Fig. 12. This time step is chosen as the time when the Fourier coefficient for the wavenumber $w = 1$ is attenuated by $1/e$. The error for the IDO scheme possesses fourth-order convergence, and the magnitude of the error is smaller than the other fourth-order schemes. For $w > 1.35$, the error becomes smaller than that of the sixth-order FD scheme.

6. Accuracy for Poisson equation

It is important to solve the Poisson equation in the case of incompressible flow analysis based on a semi-implicit method such as the Marker-and-Cell (MAC) type method [18,19]. We show the numerical accuracy for the one-dimensional Poisson equation,

$$\frac{\partial^2 f}{\partial x^2} = \rho. \tag{6.1}$$

The differentiated equation of Eq. (6.1) is required for calculating the first-order derivative:

$$\frac{\partial^3 f}{\partial x^3} = \frac{\partial \rho}{\partial x}. \tag{6.2}$$

Using the approximations (2.2) and (2.3), these equations are discretized as follows:

$$\frac{2}{h^2}(f_{j+1} - 2f_j + f_{j-1}) - \frac{1}{2h}(f_{x,j+1} - f_{x,j-1}) = \rho_j, \tag{6.3}$$

$$\frac{15}{2h^3}(f_{j+1} - f_{j-1}) - \frac{3}{2h^2}(f_{x,j+1} + 8f_{x,j} + f_{x,j-1}) = \rho_{x,j}. \tag{6.4}$$

The numerical solutions of f_j and $f_{x,j}$ can be obtained adopting relaxation procedures such as the Successive Over Relaxation (SOR) method. Sakurai et al. showed that the Multi-Grid (MG) method [20,21] effectively improves the convergence of the relaxation process and the red-black MG method is applicable to the parallel computing in the same manner as the FD scheme.

When the exact solution is assume to be Eq. (3.3), the source terms of Eqs. (6.3) and (6.4) are determined as

$$\rho_j = \sum_k -\left(\frac{w}{h}\right)^2 \hat{f}(k) e^{iwx_j/h}, \tag{6.5}$$

$$\rho_{x,j} = \sum_k -i\left(\frac{w}{h}\right)^3 \hat{f}(k) e^{iwx_j/h}. \tag{6.6}$$

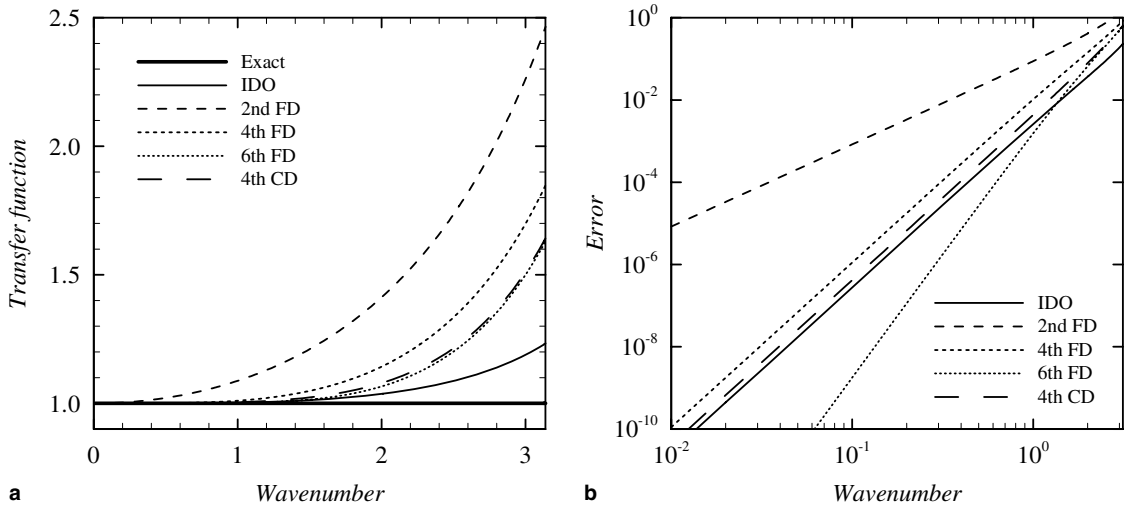

Fig. 13. Results for the Poisson equation: (a) transfer function; (b) error.

The Fourier coefficients of the numerical solutions $\hat{f}^n(k)$ and $\hat{f}^n_x(k)$ are satisfied with the following equations:

$$\left(\frac{4\cos w - 4}{h^2}\right)\hat{f}^n(k) + \left(\frac{-\mathrm{i}\sin w}{h}\right)\hat{f}^n_x(k) = -\left(\frac{w}{h}\right)^2\hat{f}(k), \tag{6.7}$$

$$\left(\frac{15\mathrm{i}\sin w}{h^3}\right)\hat{f}^n(k) + \left(\frac{-12 - 3\cos w}{h^2}\right)\hat{f}^n_x(k) = -\mathrm{i}\left(\frac{w}{h}\right)^3\hat{f}(k), \tag{6.8}$$

where Eqs. (3.8) and (3.9) are applied. These equations lead to

$$\hat{f}^n(k) = \frac{w^2(12 + 3\cos w + w\sin w)}{3(12 - 12\cos w - \sin^2 w)}\hat{f}(k) = T(w)\hat{f}(k), \tag{6.9}$$

where T is called the transfer function, which means the ratio of the numerical value to the exact one, and the exact transfer function is unity. Fig. 13(a) illustrates the transfer functions for the IDO scheme, the FD schemes, and the CD scheme. The transfer function of the IDO scheme is the closest to unity among these schemes. Fig. 13(b) shows the error for the Poisson equation, estimated by

$$E(w) = |1 - T(w)|. \tag{6.10}$$

The IDO scheme gives fourth-order accurate solutions with smaller errors than the fourth-order FD and CD schemes. The solutions of the IDO scheme are estimated more accurately than the sixth-order FD scheme for wavenumbers $w > 1.35$.

7. Conclusions

We have evaluated the accuracy and stability of the IDO scheme by using Fourier analysis. The IDO scheme is based on the Hermite interpolation functions constructed by both physical variables and spatial derivatives with compact stencil. It is unique that the derivatives are obtained by solving the additional equations derived by the differentiation of governing equations. The eigenvalues for the Runge–Kutta time integration of the IDO scheme shows stable regions for the Courant number and the diffusion number. The effective utilization of the Hermite interpolation function leads the phase speed in advection calculations to be highly accurate for high wavenumbers, even beyond the sixth-order CCD scheme. In advection calculations by the upwind IDO scheme, the numerical viscosity, which consists of the fourth- and the fifth-order derivatives, stabilizes the time integration for wavenumbers near π. Not only for the advection equation but also for the diffusion and the Poisson equations, the IDO scheme accurately resolves high wavenumbers in comparison

with other schemes. It is expected that the high resolution characteristics of the IDO scheme for all the terms of fluid flow equations is suitable for DNS of turbulent flows and also gives us better numerical results for various PDEs.

Acknowledgement

This work was partly supported by Grant-in-Aid for Scientific Research (B) from the Japan Society for the Promotion of Science.

References

[1] D. Gottlieb, A. Orszag, Numerical Analysis of Spectral Methods, SIAM, Philadelphia, PA, 1977.
[2] J. Kim, P. Moin, R. Moser, Turbulence statistics in fully developed turbulent channel flow at low Reynolds number, J. Fluid Mech. 177 (1987) 133.
[3] P. Spalart, Direct numerical simulation of a turbulent boundary layer up to $\mathrm{Re}\,\theta = 1410$, J. Fluid Mech. 187 (1988) 61.
[4] S.K. Lele, Compact finite difference schemes with spectral-like resolution, J. Comput. Phys. 103 (1992) 16.
[5] T. Yabe, T. Aoki, A universal solver for hyperbolic equations by cubic-polynomial interpolation I. One-dimensional solver, Comput. Phys. Commun. 66 (1991) 219.
[6] T. Yabe, F. Xiao, T. Utsumi, The constrained interpolation profile method for multiphase analysis, J. Comput. Phys. 169 (2001) 556.
[7] T. Utsumi, T. Aoki, T. Kunugi, Stability and accuracy of the cubic interpolated propagation scheme, Comput. Phys. Commun. 101 (1997) 9.
[8] R. Tanaka, T. Nakamura, T. Yabe, Constructing exactly conservative scheme in a non-conservative form, Comput. Phys. Commun. 126 (2000) 232.
[9] K. Takizawa, T. Yabe, T. Nakamura, Multi-dimensional semi-Lagrangian scheme that guarantees exact conservation, Comput. Phys. Commun. 148 (2002) 137.
[10] F. Xiao, A simple CIP finite volume method for incompressible flows, JSME Int. J. B 47 (2004) 664.
[11] T. Utsumi, H. Kimura, Solutions of partial differential equations with the CIP–BS method, JSME Int. J. B 47 (2004) 761.
[12] Y. Ogata, T. Yabe, Multi-dimensional semi-Lagrangian characteristic approach to the shallow water equations by the CIP method, Int. J. Comput. Eng. Sci. 5 (2004) 699.
[13] T. Aoki, Interpolated Differential Operator (IDO) scheme for solving partial differential equations, Comput. Phys. Commun. 102 (1997) 132.
[14] T. Aoki, S. Nishita, K. Sakurai, Interpolated differential operator scheme and application to level set method, Comput. Fluid Dynam. J. 9 (4) (2001) 418.
[15] T. Aoki, 3D simulation for falling papers, Comput. Phys. Commun. 142 (2001) 326.
[16] T. Kobara, T. Aoki, M. Tanahashi, Interpolated Differential Operator (IDO) scheme for direct numerical simulation of two-dimensional homogeneous isotropic turbulence, Trans. JSME B 70 (2004) 2791 (in Japanese).
[17] P.C. Chu, C. Fan, A three-point combined compact difference scheme, J. Comput. Phys. 140 (1998) 370.
[18] F.H. Harlow, J.E. Welch, A numerical calculation of time dependent viscous incompressible flow of fluid with free surface, Phys. Fluids 8 (1965) 2182.
[19] A.A. Amsden, F.H. Harlow, A simplified MAC technique for incompressible fluid flow calculations, J. Comput. Phys. 6 (1970) 322.
[20] K. Sakurai, T. Aoki, W.H. Lee, K. Kato, Poisson equation solver with fourth-order accuracy by using interpolated differential operator scheme, Comput. Math. Appl. 43 (2002) 621.
[21] M.C. Thompson, J.H. Ferziger, An adaptive multigrid technique for the incompressible Navier–Stokes equations, J. Comput. Phys. 82 (1989) 94.